First publ. in: Phase transitions in surface films [proceedings of the NATO Advanced Study Institute and International Course on Phase Transitions in Surface Films, held June 19 - 29, 1990, in Erice, Sicily, Italy], 1991, pp. 135-151

NEUTRON SCATTERING STUDIES OF QUANTUM FILMS

H.J.Lauter, H.Godfrin, V.L.P.Frank and P.Leiderer*

Institut Laue-Langevin, BP 156X, F-38042 Grenoble, France
*Institut fur Physik, Universitat Konstanz, D-7750 Konstanz,FRG

INTRODUCTION

The phase diagrams of a monolayer of adsorbed gases or light molecules on flat substrates look similar to the phase diagrams in 3-dimensions (3-D). This means that the usual coexistence regions, the triple point and the critical point are present as well in 2-dimensions (2-D) as in 3-D [1]. The phase diagrams can be studied by adsorption isotherm or heat capacity measurements, which reveal mainly the coexistence regions or the phase boundaries, respectively. However, the substrate can not always be regarded to be ideally flat. In many cases the adsorbate does see the adsorption sites of the substrate and locks into a commensurate phase (C-phase). In the case of graphite as substrate the ($\sqrt{3}$ x $\sqrt{3}$) R 30° overstructure is seen in many cases. This structure is shown in fig.1. The heavier rare gases and the light molecules (N_2, CD_4) exhibit the C-phase only if the lattice parameter of the dense plane in 3-D is close to the nearest neighbor distance in the C-phase. This is the case because the nearest neighbor distance nearly does not change in the densest plane if the adjacent planes are taken off which means the dimensionality changes from 3-D to 2-D. The quantum gases however all show a C-phase in their 2-D phase diagram despite a much

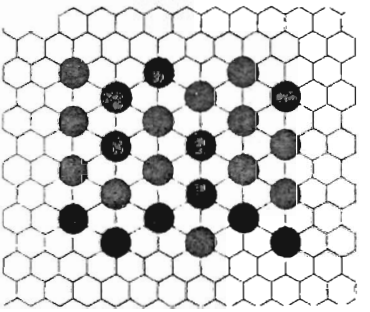

Fig.1: Model of the commensurate ($\sqrt{3}$ x $\sqrt{3}$) R 30° overstructure on graphite.

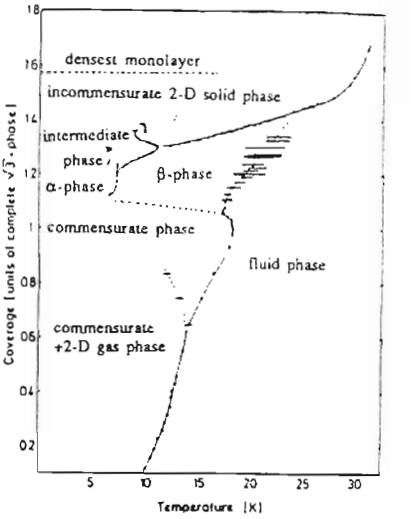

Fig.2: Phase-diagram of D_2 on graphite [2].

denser nearest neighbor distance in 3-D. This is due to the zero-point motion which gives a repulsive contribution to the nearest neighbor interaction and consequently a high compressibility to the system. Thus if as before the dimensionality is changed and many of nearest neighbor atoms are missing the 2-D lattice expands. If in addition the corrugation of the adsorption potential is added, the quantum gases recognize the dilute density structure of the C-phase as the ground state.

The phase diagram of D_2 on graphite is shown in figure 2 as an example of an adsorbed quantum gas. The location of the phase boundaries has been determined by heat capacity measurements [2]. The definite allocation of the different phases to structures is given by scattering techniques. In this case it has been done by neutron diffraction and LEED [3,4].

The inelastic neutron scattering gives additional information of the interaction between the adsorbed particles itself but also between the adsorbate and the substrate. In particular interesting is the search for the phonon gap at the zone center which characterizes the loss of the translational invariance of the adsorbed layer in the C-phase. The transition from the C-phase to the incommensurate higher density phase is characterized by different intermediate phases as seen in figure 1. Theories of the commensutrate-incommensurate transition predict domain walls in the transition region. In these domain wall phases the commensurate phase is still locally present. Thus the study of the phonon gap will reveal interesting features.

EXPERIMENTAL

The experimental set-up is described in Ref.5. The sample consists of a stack of exfoliated graphite sheets (Papyex) with a diameter of 2 cm and a height of about 7 cm. The surface area is in the order of 200 m^2. The graphite is a 2-D powder. Only the axis perpendicular to the basal planes of the graphite shows a certain order of a mosaicity of about 30° FWHM. The coherence length of the adsorbed layer is about 300 Å in the C-phase. The basal planes of the graphite are parallel to the scattering plane of the neutron spectrometer. For the inelastic studies the IN3 spectrometer of the ILL has been used with a fixed final energy of 1THz and a Be-filter on the analyser end. The resolution across the elastic line was 0.03THz. For the elastic studies ZYX-graphite was used with a coherence length of about 2000 Å.

The density of the adsorbate was controlled by adsorption isotherms. But also the highest intensity of the Bragg-peak of the adsorbate in the C-phase as a function of coverage at constant temperature determines the best commensurate phase $\rho=1$. $\rho=1$ means that all adsorption sites in the C-phase are occupied by adsorbed atoms or molecules. The definition of $\rho=1$ with diffraction is within 2-3% identical with the $\rho=1$ coverage defined by the highest melting temperature of the C-phase in figure 2. The small difference may be a real temperature effect.

MEASUREMENTS

I. THE ($\sqrt{3} \times \sqrt{3}$) PHASE

The verification of the C-phase has to be done by diffraction. In fig.3 neutron diffraction patterns are shown at various average adsorbate densities [3]. The spectrum A at a slightly overfilled C-phase shows the maximum intensity at a momentum transfer $Q=1.702$ $Å^{-1}$ which corresponds for a triangular lattice to 4.26 Å, the nearest neighbor distance in the C-phase (fig.1). All the spectra shown, the elastic and the inelastic ones, show difference counts. The signal from the cell and substarte without adsorbate has always been subtracted.

The inelastic neutron measurements have been taken at two different momentum transfers Q. The reason for that is depicted in fig.4 which shows the reciprocal space of the triangular lattice of the C-phase. The scan taken with a $Q=1.7$ $Å^{-1}$ collects all excitations with wave vector q along the circle with radius Q with the help of the Bragg-points which are marked by the vector τ. These excitations with wave vector q have mainly transverse polarization and the highest intensity is expected from the zone boundary phonons because of the high density of

states. If a phonon gap exists at the zone center a second high density of states is expected at this point. As the 2-D powder averaging crosses also the Γ-points a second peak is expected in energy in the scan with a Q=1.7 $Å^{-1}$.

The scan taken with Q=0.85 $Å^{-1}$ collects the longitudinal zone boundary phonons due to the 2-D powder averaging (fig.4). So with the correct choice of the momentum transfer different modes can be separated even in a powder-like sample.

The scans with the different momentum transfers are shown in figure 5. The data points in fig.5a (Q=1.7 $Å^{-1}$) show clearly a double peak. The one at lower energies represents the phonon gap, whereas the one at higher energies shows the collected transverse zone boundary phonons. The scan with a Q=0.85 $Å^{-1}$ (fig.5b) shows only one peak which results from collected longitudinal zone boundary phonons. The fit to the data is a two

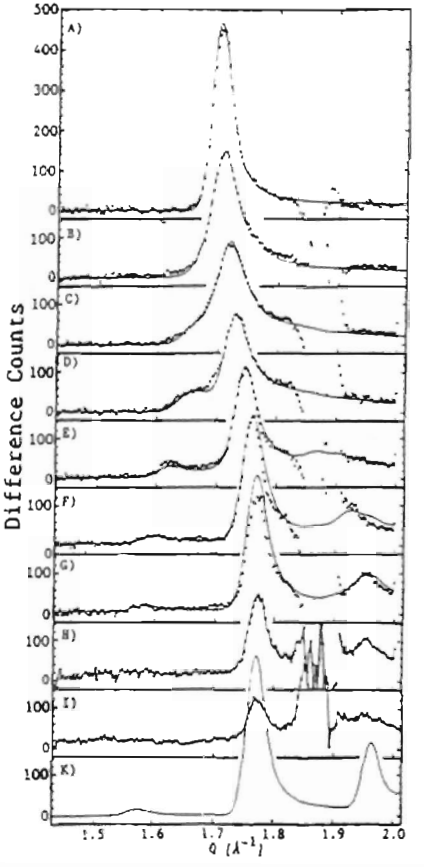

Fig.3: Diffraction pattern of D_2 on graphite in the C-phase and α-phase at various average densities of the adsorbate; A) ρ=1.07, B) ρ=1.10, C) ρ=1.11, D) ρ=1.13, E) ρ=1.16, F) ρ=1.20, G) ρ=1.23, H) ρ=1.24, I) ρ=1.25; T=2K. The solid lines are fits with the model in fig.7 [3].

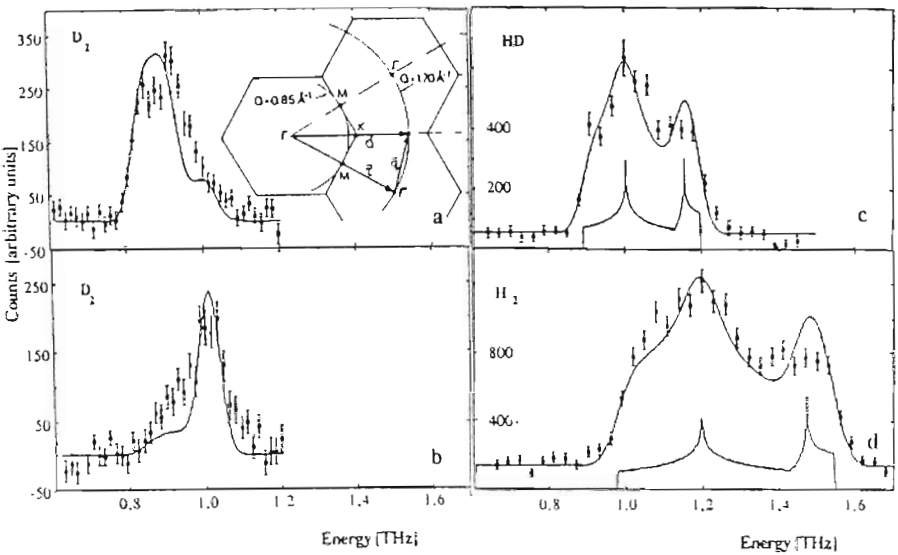

Fig.4 and fig.5: Fig.4 is the inset in fig.5a. Fig.4 shows the reciprocal space of a triangular lattice. The circles are shown on which phonons are collected due to the powder averaging for $Q=1.7$ Å^{-1} and $Q=0.85$ Å^{-1}. Q is the total momentum transfer: τ is a reciprocal lattice vector and q is the phonon wave vector [3]. Fig.5: Neutron inelastic data of the hydrogen isotopes adsorbed on graphite in the C-phase [8]. $Q=0.85$ Å^{-1} in b and $Q=1.7$ Å^{-1} in a,c and d. In a and b the spectra taken with D_2 are shown, which is a coherent scatterer. Whereas in c and d HD and H_2 is used, respectively, which are incoherent scatterers for neutrons. So the density of states is measured.

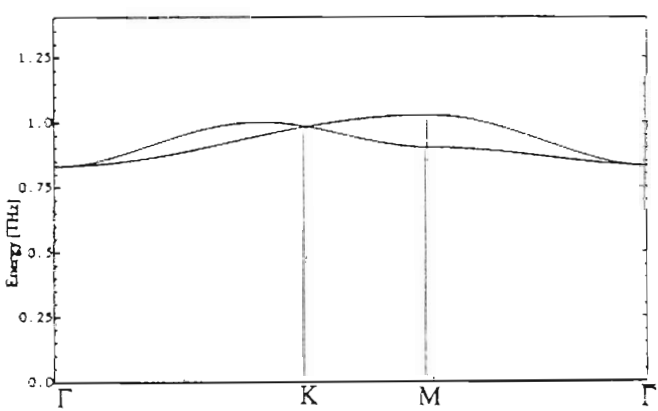

Fig.6: Calculated dispersion relation for D_2 on graphite in the C-phase [5].

parameter fit. The adsorbate molecules are thought to be connected by each other by a net of springs and each molecule is connected by a spring to the substrate [5]. The model is a very simple one and is not able to reproduce the clear separation between the phonon gap and the transverse zone boundary phonons seen in the data (fig.5a). But it is however interesting to note the difference in the spring constants. α is the spring constant between the adatoms and

Table 1: Parameters obtained from the fits characterizing the density of states for the in-plane modes of the C-phase of the hydrogen atoms adsorbed on graphite. In parenthesis are given the values of Ref.7.. Indicated are the following: z.c.gap is the zone center gap energy, width is the width of the density of states, trans.peak and long.peak are the peaks arising from the transverse and longitudinal phonons in the density of states, respectively. All values are in Kelvin (48 K = 1THz = 4.14 meV). (The experimental data of fig.5a suggest a value of 43.3K for the transverse peak)*

	H_2	HD	D_2
z.c.gap	47.3 (46.6)	43.2	40.0 (36.9)
width	27.5 (42.1)	14.7	9.5 (14.8)
trans.peak	57.9 (64.9)	48.8	43.3*(44.2)
long.peak	71.4 (83.8)	55.8	48.1 (50.3)

Table 2: Parameters that characterize the adsorbate - graphite system in the commensurate phase for Kr[11], CD_4[12], N_2[13], D_2[2], HD and H_2[3] and ^3He[14], the adsorbates are ordered with increasing de Boer parameter.

[a] The de Boer parameter indicates the quantum character of the adsorbate.

[b] This column presents the width of the in-plane phonon density of states (DOS). These values are not always easy to determine with inelastic neutron scattering, since the intensity of the structure factor decreases with increasing energy.

[c] The phase diagrams of Kr, N2 and CD4 present a commensurate phase region that extends to higher temperatures, when the total coverage is slightly higher than the commensurate one. Details of the phase diagrams can be found in refs.15, 16 and 17, respectively.

Adsorbate	Mass [a.u.]	de Boer[a] parameter	Lennard-Jones parameter		Gap energy [K]	Gap ratio $\Delta_{max}/\Delta_{peak}$	DOS width[b] [K]	Melting Temperature
			ϵ [K]	σ [Å]				
Kr	83.8	0.10	165.3	3.63	8.7	1.0	-	~125[c]
CD_4	20.0	0.23	137.0	3.68	14.5	0.9	48	~55[c]
N_2	28.0	0.42	35.6	3.32	19.3	1.7	34	~72[c]
D_2	4.0	1.26	35.2	2.95	40.0	1.1	9.5	18.5
HD	3.0	1.43	35.9	2.95	43.2	1.1	14.7	19.4
H_2	2.0	1.74	36.7	2.95	47.3	1.0	27.5	20.5
^3He	3.0	3.10	10.2	2.56	10.9	0.3	40	3.05

β the in-plane one between the adsorbate molecule and the substrate at the adsorption site. α has been determined to 0.016 N/m and β to 0.182 N/m. The ratio is about 1/10. This small ratio is equally well seen in the rather flat dispersion in fig.6. Thus the molecule exhibits nearly "Einstein behavior" [6], but the influence of adatom-adatom interaction is still visible through the dispersion. Calculations [7] are in good agreement with the value of the energy of the phonon gap, however the adatom-adatom interaction visible by the width of the density of states is still by a factor of 1.5 too small (see table 1). This indicates that probably not the parameters at the minimum of the interaction potential have to be modified but the shape of this potential at a larger intermolecular spacing due to the increased intermolecular spacing in the C-phase.

The effect of the isotope mass can be probed by using in addition to D_2 also HD and H_2 as adsorbate [8]. The spectra are shown in fig.5c and 5d. Both spectra make use of the incoherent scattering cross section of HD and H_2. The calculated density of states is seen as a solid line in the lower part of the figures. The line through the points is the density of states folded with the resolution of the instrument. The characteristic values of the dispersion relations are summarized in table 1. The same model as described for D_2 has been applied to the other isotopes. The theory [7] describes well the isotope shift which is not only due to the different mass but also due to the anharmonicity of the potentials. The isotope effect is seen with decreasing mass as well in the shift of the phonon gap to higher energies as in an increasing width of the density of states. As with D_2 the width of the density of states is wider by the same factor 1.5 (table 1).

The C-phase has also been detected for other adsorbates and a collection of gap energies and widths of the density of states is given in table 2 [9,10]. The gap energy is related to the curvature of the corrugation of the in-plane adsorption potential at the adsorption site. The agreement between theoretical calculations of the gap energy and the measured values is indicated in the 7th column of table 2 [7,9,10,18]. The effective curvature is influenced by the movement of the atoms or molecules in the adsorption potential. All the quantum gases are governed by the zero point movement, so that the gap stays nearly unchanged up to the melting temperature of the C-phase. Kr and CD_4, however, show a lowering of the gap energy by a factor of 2 when the temperature is raised to the melting.temperature due to the enhanced mean-square displacement of the adsorbate and the anharmonicity of the adsorption potential [9,19,20].

Also the width of the density of states exhibits the difference between the quantum gases and the heavier gases. The quantum gases show a smaller width of the density of states, because the nearest neigbor distance in the C-phase is increased with respect to the one in 3-D. This leads to a lower interaction between adsorbate atoms. The heavier gases show more interaction, because the nearest neigbor distance in 3-D matches the one in 2-D. The high value of ^3He should be taken with care. On one side the very high zero point motion may allow for a higher adsorbate-adsorbate interaction, but on the other side we are not absolutely sure about the interpretation of the data [14].

II. THE COMMENSURATE-INCOMMENSURATE TRANSITION

Once the inelastic signals are understood in the C-phase the adjacent phases can be investigated. This will be described first for the α-phase. In fig.3 several scans are shown taken at different coverages and constant temperature. They follow a path from the C-phase into the α-phase (fig.2). The diffraction peak shifts with increasing density to higher Q-values according to the compression. At the same time satellites are moving outwards from the main peak. The feature around 1.88 $Å^{-1}$ is the (002) graphite peak, which is due to an interference phenomena. It is of no importance for this study and cuts unfortunately out a

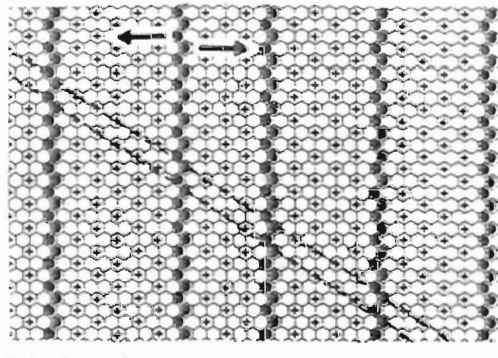

Fig.7: Striped superheavy domain wall model for D_2 on graphite [3].

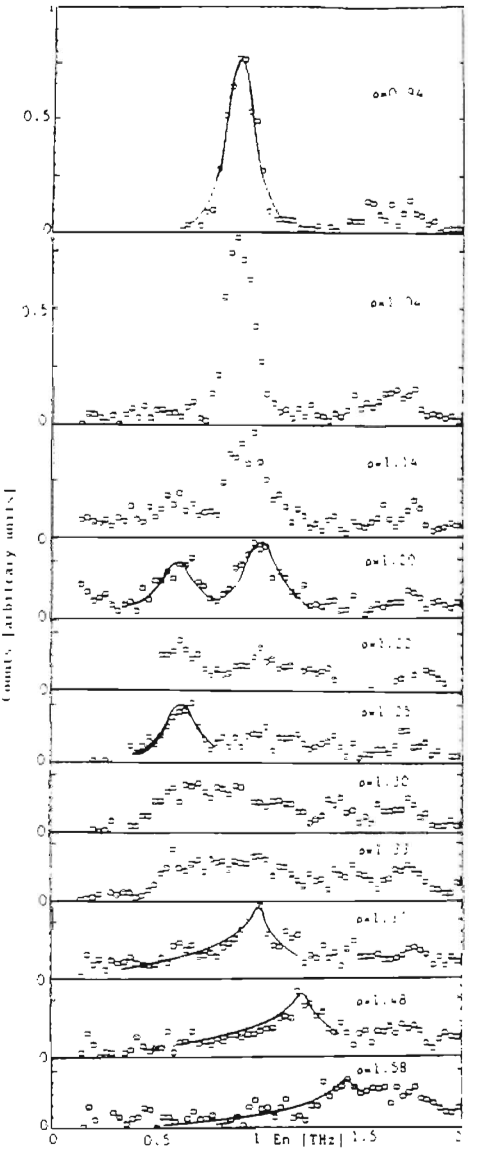

Fig.8: Neutron inelastic data of D_2 on graphite at T=4K for various coverages (Q=1.7 $Å^{-1}$) [9]. The lines are guides to the eye.

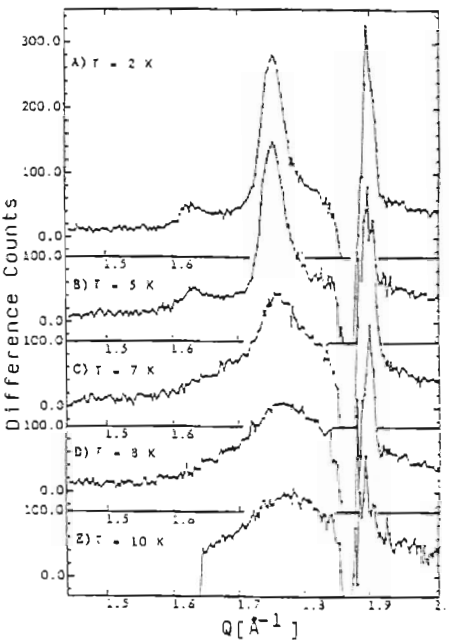

Fig.9: Diffraction pattern of D_2 on graphite at constant coverage ρ=1.16 (see fig.2) at various temperatures showing the α-β transition between 5K and 7K[3b].

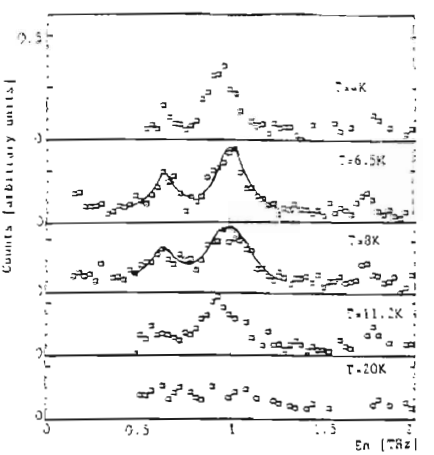

Fig.10: Neutron inelastic data of D_2 on graphite at constant coverage ρ=1.16 (see fig.2) at various temperatures across the α-β transition [9]. The lines are guides to the eye.

certain region in Q, where the signal of the adsorbate is not observable. The fit to the data has been done with a model of striped superheavy domain walls [3,4] which is depicted in fig.7. For a more detailed discussion the reader is referred to the Refs.3 and 4. It should only be mentioned that the crosses in fig.7 represent the molecules still in the commensurate position. The filled circles mark the molecules in the domain walls in an ideal position. However they are too close and a certain relaxation indicated by the arrows takes place. In the applied model the distance between the domain walls has a distribution which depends on the domain wall density. The width of the domain walls is fairly small. It extends only across 4 rows of molecules. This is again due to the high compressibilty of the 2-D quantum gases as mentioned in the introduction.

The inelastic study of the domain wall structure is shown in fig.8 [21]. The top two spectra are taken in the C-phase and show the phonon gap and the transverse zone boundary phonon in one peak due to the relaxed instrument resolution (0.06 THz) used for these scans. If the average density is further increased the α-phase is entered (see fig.2) and the signal around 1 THz starts to decrease. This is understood as due to the amount of the molecules in the C-phase decreasing due to the model of the domain walls. At the same time a signal at about 0.6 THz appears which finally at ρ=1.25 is the only signal to be seen. This signal attributed to an excitation of the domain walls is still to be calculated. It is best at the densest α-phase (ρ=1.25, see fig.2). This is a first example of the usefulness of the inelastic studies to complete and to understand the events in this phase diagram.

The following scans in fig.8 show that in the region between ρ=1.30 and ρ=1.33 the signals can not be any more resolved probably due to too many different excitations in this phase which was modeled by a hexagonal heavy domain wall structure [3,4]. In the region beyond the density of ρ=1.33 the inelastic response changes again and indicates the pure transverse zone boundary phonon of an incommensurate 2-D solid.

The next object to study is the β-phase. In fig.9 diffraction patterns are shown taken at constant coverage ρ=1.16 as a function of temperature [3]. At T=2K and 5K the already known satellite structure of the α-phase is seen, which could be modeled by striped superheavy domain walls. For higher temperatures than the α–β transition (fig.2) the spectrum looks like a liquid structure factor in particular if the temperature is raised. The structure of this "reentrant liquid" was not known, but got new interest because this phase seems to be separated from the normal 2-D liquid by very broad peaks in specific heat (fig.2). The inelastic neutron measurements are shown in fig.10. They have also been taken with the relaxed resolution (fig.8). So again the excitations of the commensurate parts (phonon gap and transverse zone boundary) are seen and at lower energy the signal from the domain walls. Here no change in the spectrum is seen if the temperature crosses the α–β transition at 7.2 K. The consequence is that the domain walls do still exist in the β-phase because the excitation belonging to them are still visible and also the excitations from a commensurate phase. The solution for a structural picture is to introduce patches of domain walls as depicted in fig.11. This model still allows for the inelastic features and the structure factor, seen as inset in fig.11 [3b], fits the data. This is a proof that the β-phase is a disordered domain wall phase. The evolution with temperature can be modeled by shorter and shorter domain walls until melting around 20K. Perhaps the unbinding of domain walls can be treated in the class of Kosterlitz-Thouless transitions [22,23].

The phase diagram of the monolayer of the heliums adsorbed on graphite are similar to the ones of the hydrogens in that a pronounced C-phase shows up with a transition to the incommensurate phase probably via a striped superheavy domain wall phase [24-26]. We present here the identification of the domain wall (D) phase of ^{3}He as a striped superheavy domain wall phase.

In fig.12 the explored coverage range between 0.05 and 0.35 atom/Å^2 of ^{3}He on graphite is shown. The density of the adsorbed layer can be calculated from the diffraction peak position if a homogeneous triangular lattice is assumed. The first five points in fig.11 show all the same ordinate of 0.0636 at/Å^2, the density of the C-phase. The abscissa's calibration (the total number of adsorbed atoms on the surface of the sample) is given by the amount of

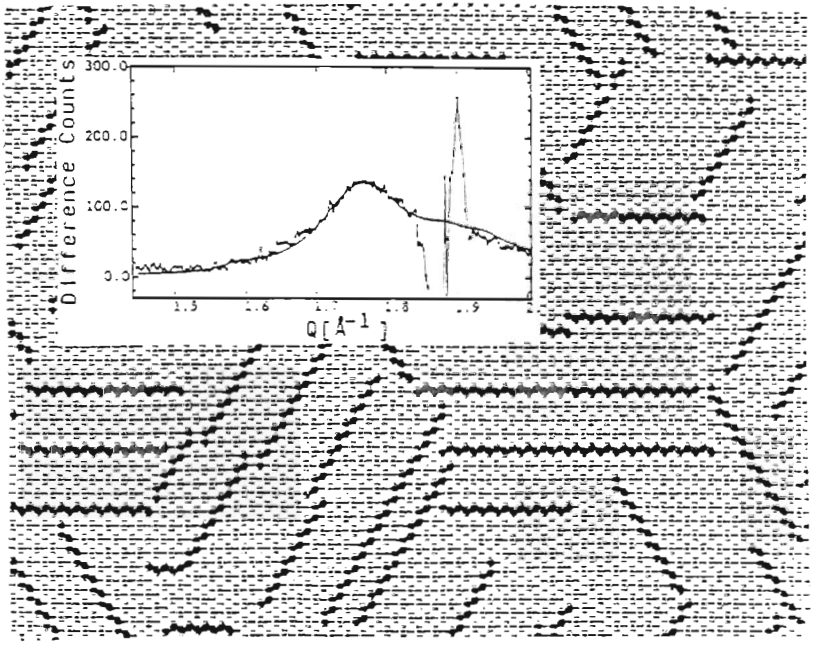

Fig.11: Model for the β-phase. It is made up of patches of the α–phase structure [3b]. The inset shows an overlay of a measured spectrum in the β-phase (spectrum c in fig.9) and calculated one using the structure from the same figure [3b].

^{3}He that produces the highest Bragg-peak intensity within the C-phase. This defines the best C-phase: all adsorption sites of the C-phase on the graphite are occupied by an adsorbate atom. This calibration was first made with D_2 on graphite [3] and defined a value of 14.34 cc (STP) of gas. This agrees with ^{3}He, despite its low scattering power and high neutron absorption cross section.

The straight full line in fig.12 through the best C-phase point and the origin does not match the points in the IC1-phase. This shows clearly that the calibration of the C-phase and of the incommensurate (IC1) phase do not coincide. One possible explanation is that the effective surface area of the C-phase is smaller than the one of the IC1-phase. Another possibility may be that in the IC1-phase atoms are additionally adsorbed on other planes than the basal ones. The calibration of the IC1-phase is shown in fig.12 by the dashed line, which does not pass through the origin. The difference at monolayer completion amounts already to 6% .

The deduced densities in the D-phase (fig.2) show a behavior that is equivalent to the case of D_2 [3,4], which has been identified as a striped superheavy domain wall phase. The much less favorable scattering conditions of ^{3}He with respect to D_2 made it impossible to measure any satellites. However, the characteristic coverage dependence in fig.12 is a proof that this domain wall phase exists as proposed by heat capacity measurements for ^{4}He [25]. The density deduced from the diffraction peak position does of course not represent any more the real density of the layer, but serves just for visualization. The densest stage is reached when the superheavy walls are separated by one row of atoms in commensurate position (7) as for D_2 [3,4].

III. THE SECOND ADSORBED LAYER

For the helium isotopes, the second adsorbed layer is less dense than the first one [27] in contrast to the hydrogen isotopes [28], where both layers have the same density. The weaker adsorption potential and the enhanced zero point motion of the helium atoms are clearly visible in the low density of the second layer. Under the pressure of the second layer the density of the first layer increases slightly and finally locks into a 8*8 and 9*9 overstructure for ^{3}He and ^{4}He [3b], respectively.

The second layer promotion is evidenced as a sharp knee between the IC1 and IC2-phase in fig.12. The increasing pressure of the second layer on the first one induces a further compression of the first layer, seen by the small slope in the IC2-phase. This slope increases slightly towards the S-phase, changing over to a zero slope at 0.2 at/Å^2. At this point the density of the first layer (0.1106 at/Å^2) corresponds to an 8*8 overstructure with respect to the graphite, having 37 atoms per unit cell. The approach to this clear lock-in is marked in the S-phase by some diffraction peaks, whose line shape is better described by a double peak. This splitting is shown in the insert of fig.12. It can be interpreted as a slight distortion of the unit cell due to a one directional registry with the substrate. This partial registry agrees for two points with the 4*4 lattice spacing and for one point with the 8*8 one, before finally the pure 8*8 overstructure is reached.

The diffraction of the second layer itself could be seen only at higher coverages around a total density of 0.3 at/Å^2 (fig.12)
Similar features in the bilayer region are seen for ^{4}He on graphite in fig.13 [3b]. For intensity reasons the signal from the C-phase could not be seen. Thus only the peak positions from the IC1-phase (see fig.12) appear at low densities. For the same reason we could not calibrate the x-axis on the best C-phase as was done in fig.12. Thus the x-axis is in square root of the amount of the filling. The substrate used is Papyex with a coherence length of about 350 Å. But in addition the data obtained with ZYX-substrate (coherence length about 2000 Å) are shown in fig.13 with a rescaling at the monolayer completion for the x-axis.

Again the second layer promotion is evidenced as a sharp knee at a density of 0.112 at/Å^2 (^{3}He at 0.106 at/Å^2 in fig.12) and the increasing pressure of the second layer induces a small further compression of the first layer. At a filling of 19 cc$^{3/2}$ the first layer locks into an

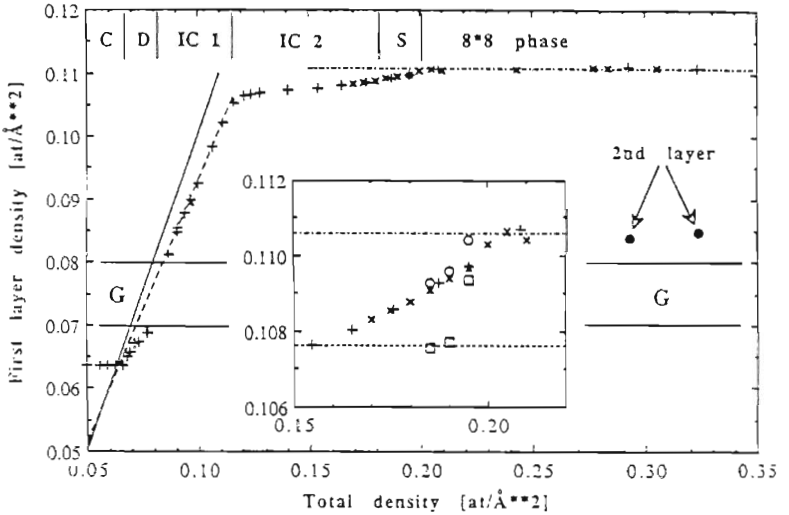

Fig.12: Measured density of the first ^{3}He layer vs. total coverage at T=1.0K (+) and at T=0.06K (x). (□) and (o) indicate the splitting of the diffraction peak in the insert. (•) is the position of the second layer density. The identification of the different phases is described in the text. G marks a region disturbed by a graphite background reflection. The full and dashed line depict the monolayer behavior. The dashed-dotted line shows the density of the 8*8 phase. The dashed line (insert) indicates the 4*4 density

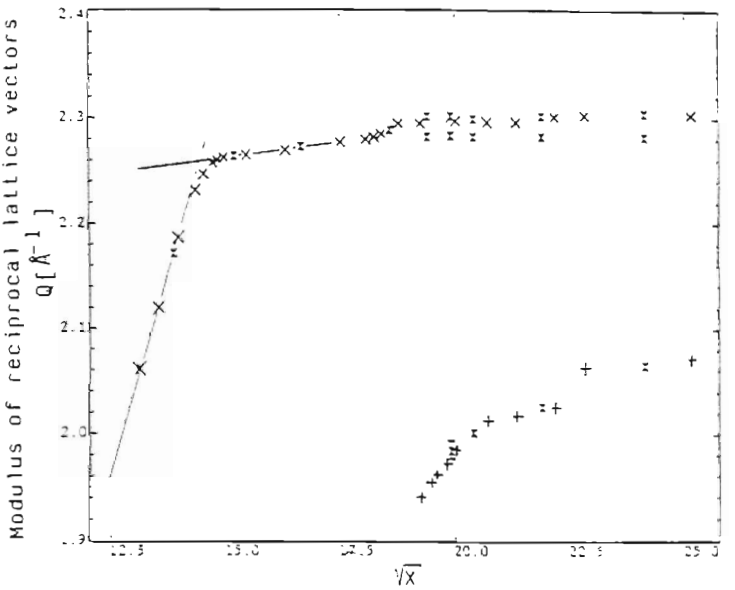

Fig.13: Measured reciprocal lattice vectors for ^{4}He adsorbed on Papyex (x) at T=1.2 K as a function of the square root of the total coverage taken in units of cm^3 STP (√X). (×) and (+) are the ZYX data, rescaled to the coverage at the monolayer completion for the Papyex sample.

overstructure with respect to the graphite. This time it is the 9*9 overstructure for the ZYX- substrate. For the Papyex a splitting of the diffraction peak is observed, which indicates a one directional registry with the substrate induced by the small coherence length of this substrate.

The second layer diffraction peaks become visible at a filling of 19 $cc^{3/2}$ and a compression of the second layer density is seen with the third layer promotion in fig.13.[36]

IV. THE ^{4}HE FILM

A ^{4}He film on graphite is composed of two solid layers adjacent to the substrate (below 2K) and subsequent liquid layers (see e.g.Ref.13). So the liquid ^{4}He film has two boundaries,

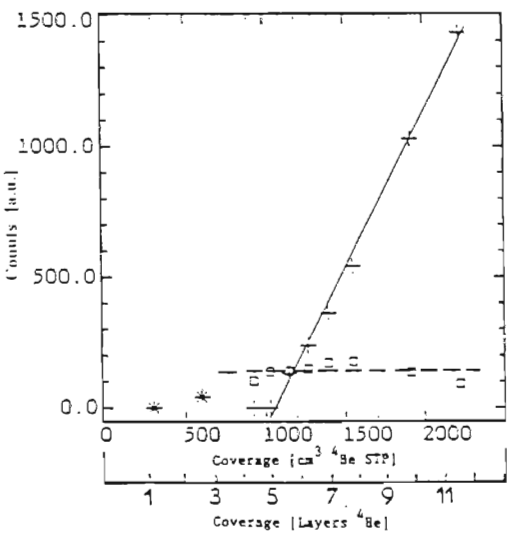

Fig.14: Intensities of the bulk signal (+) and the interface signal (o) at the energy of 0.6 meV as a function of coverage (^{4}He on graphite powder [31]). The signal at a coverage of a monolayer and at 2.6 layers is marked by (*) (it is a constant background !); T=0.8K.

the solid-liquid one and the liquid-gas one. Excitations can propagate along these interfaces, which are the freezing-melting wave [29] and the ripplon [30], respectively. Any excitation with a dispersion like a freezing wave could not yet be measured with neutron scattering. But in addition to the signals arising from the bulk ^{4}He some modes could be detected which have no dispersion (the energy does not change as a function with wave vector). These modes (at 0.4 meV, 0.6 meV....) are localized at the solid-liquid interface because they still exist if the sample cell is completely filled with helium (this means that the liquid-gas interface is suppressed) [31]. On the other hand these modes disappear between a coverage of 2.5 and 4

layers as shown in fig.14. This range has unfortunately not been investigated in more detail. But for coverages beyond 4 the intensity of this mode does not increase as function of coverage in agreement with the explanation that it is bound at the solid-liquid interface. These modes can be taken to explain the high transmission of phonons through the interface between a soilid and liquid helium (Kapitza-resistance). In contrast the bulk signal increases linearly with coverage. It extrapolates to zero at a coverage of 5 layers. This indicates that in addition to the two solid layers three liquid layers do not contribute to superfluidity, if superfluidity is connected to the measurability of the phonon-roton dispersion curve.This statement will be refined for the 4He film on Payex-graphite, which is described in the following.

At the second interface a ripplon should be visible. Indeed it could be measured [31-33] and shows the dispersion expected from theory [30]. The attribution of this mode to be a ripplon was strengthened by the fact that this mode disappears if the liquid-gas interface is suppressed by filling the sample cell completely with helium. This is visualized in the figs. 15 and 16. In the figures the different colors indicate the behavior of the intensity as a function of energy and momentum transfer. It is clearly seen in fig.15 that besides the intensity on the phonon-roton curve there is intensity on an energetically lower lying branch. This branch coincides with the calculated dispersion of the ripplon using the parameter set in Ref.20. The agreement is very good, it seems to be so even up to 1.5Å-1. At still higher Q the roton intensity combined with the one of the flat modes becomes to high to distinguish the ripplon signal. This good agreement allows to say that the temperature dependence of the surface tension is really based on an experimentally verified dispersion relation. It still remains to prove the modified parameter set [30] by a theory.

In fig.16 the result of the completely filled sample cell is shown. In the region where the ripplon should show up, the colors are the same as in fig.15. Only near the phonon-roton intensity and the flat bar due to the multiple scattering [31,32] the attribution of the colors to intensity has been modified. Thus this figure shows that no signal of the ripplon intensity is visible in fig.16 the filled cell data, although below 0.7 $Å^{-1}$ it would have been distinguishable from the overwhelming quasi bulk phonon roton intensity. This disappearance proves that the ripplon signal is really bound to the gas-liquid interface.

The fig.17 shows the evolution of the signal height of the ripplon with coverage. Again the saturation shows that this mode is bound to an interface. It becomes visible above 3 layers (two of them solid !). Like in fig.14 the evolution of the bulk signal is exhibited. The extrapolation is made only with coverages below 5 layers. This shows that the bulk signal disappears at about 3.5 layers. There is no discrepancy with the dependence in fig.14 because here in fig.17 the scale is much finer and in principle a linear tail of the bulk signal height as a function of coverage is seen. (A rough extrapolation from still higher coverages extrapolates to about 4.5 layers in agreements with fig.14.)

In conclusion it has been shown that a lot of information can be drawn from adsorbates even on powder like graphite substrates using elastic and inelastic neutron scattering. These studies give insight into the dynamical behavior of the adsorbates in the commensurate phase itself, but which is also very valuable for the modelling of 2-D phases in the demonstrated case of the commensurate-incommensurate transition. All the adsorbed quantum gases have a commensurate-incommensurate transition, where the striped superheavy domain wall phase appears as intermediate phase. This domain wall phase shows again phase transitions as a function of temperature which implies the creation of shorter pieces of domain walls. The evolution of the first layer structure is demonstrated towards the densest monolayer and under the pressure of the second layer. Due to the second layer pressure the first layer of the helium show overstructures with the substrate. In particular interesting are the interface excitations of an ^{4}He film. At the solid-liquid helium interface localized excitations could be detected and at the liquid-gas helium interface the ripplon could be measured. Thus an overview has been given what can be measured with neutron scattering in the case of adsorbed quantum gases on graphite ranging from a submonolayer to a film.

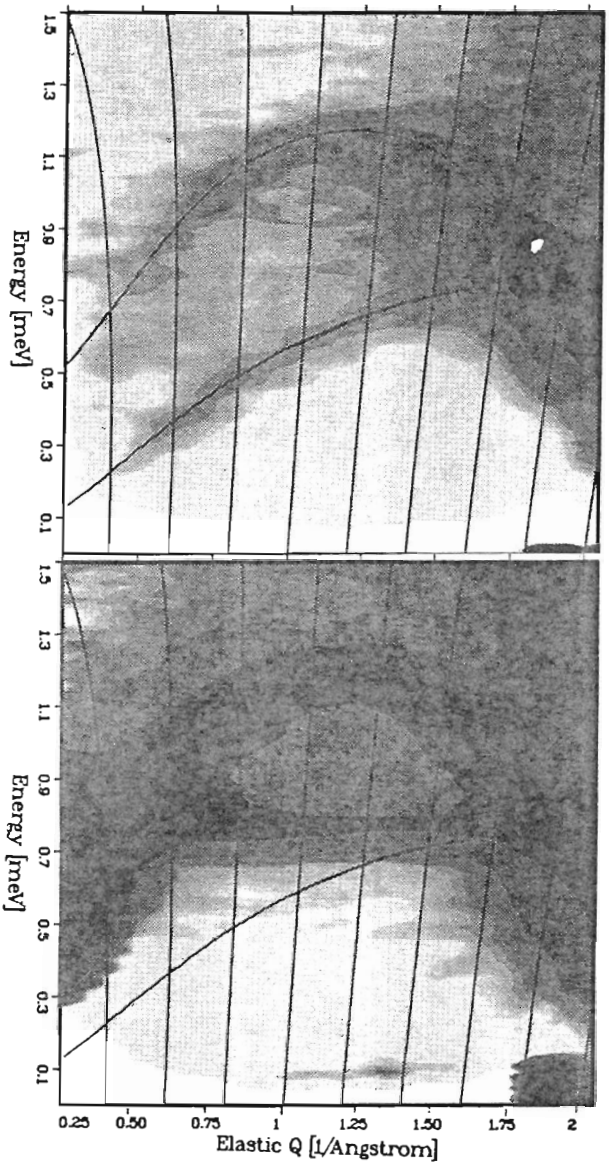

Fig.15 (top)and 16 (bottom): Intensity along the phonon-roton curve and along the ripplon curve in the energy-Q plane. The intensities originately displayed as different colors are visualized by the graduation from white to black,which marks the highest intensity (e.g. at the roton minimum in fig.15). Fig.15 shows the signal from 5.06 adsorbed layers on Papyex and fig.16 the signal from the completely with ^{4}He filled sample cell. In both figures the phonon-roton curve of bulk helium is seen as a black line as well as the ripplon dispersion.

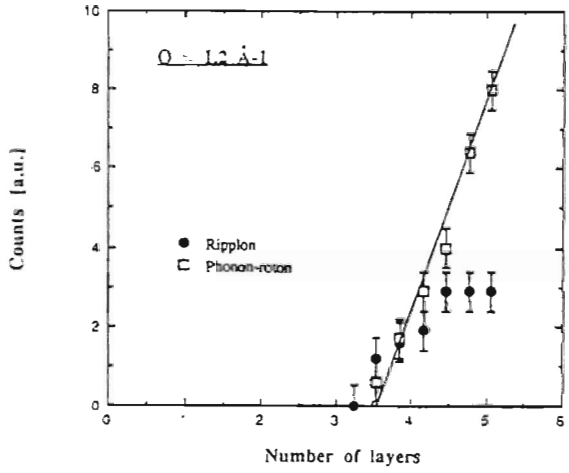

Fig.17: Intensities of the bulk signal (o) and the ripplon (●) as a function of coverage (^{4}He on Papyex-graphite); T=0.6K.

ACKNOWLEDGEMENTS

This work has been partially supported by the Federal Ministry of Research and Technology (BMFT), F.R.G.

REFERENCES

1. Thomy A., Duval X. and Regnier J., Surf.Sci.Rep.1, 1 (1981)
2. Freimuth H. and Wiechert H., Surf.Sci. 178, 716 (1986)
3a.Schildberg H.P., Lauter H.J., Freimuth H., Wiechert H. and Haensel, Jap.J. Appl. Phys.26, 345 (1987),(Proc.18th Int.Conf.on Low Temperature Physics, Kyoto);
3b.Schildberg H.P., Thesis, University of Kiel R.F.A. (1988)
3c. H.J.Lauter, in "Phonons 89", Hunklinger. S., Ludwig W. and Weiss G.edts.(World Scientific, 1990) p.871
4. Cui J., Fain S.C., Freimuth H., Wiechert H., Schidberg H.P. and Lauter H.J., Phys.Rev.Lett.60, 1848 (1987)
5. Frank V.L.P., Lauter H.J. and Leiderer P., Phys.Rev.Lett.61, 436 (1988)
6. Nielsen M., McTague J.P. and Passell L, Phase Transitions in Surface Films, Plenum Press (1980) p.127
7. Novaco A.D., Phys.Rev.Lett.60, 2058 (1988)
8. Lauter H.J., Frank V.L.P., Leiderer P. and Wiechert H., PhysicaB156&157, 280 (1989)
9. Lauter H.J., Frank V.L.P., Taub H. and Leiderer P.,LT-19, PhysicaB165&166, 611 (1990)
Frank V.L.P., Lauter H.J., Godfrin H. and Leiderer P., NATO Workshop, Exeter 1990
10 Bruch L.W. same NATO Course
11 Frank V.L.P., Lauter H.J. and Taub H., unpublished data
12 Moeller T., Lauter H.J., Frank V.L.P. and Leiderer P., "Phonons 89", Hunklinger. S., Ludwig W. and Weiss G.edts.(World Scientific, Singapore 1990) p.919
13 Hansen F.Y., Frank V.L.P., Taub H., Bruch L.W., Lauter H.J. and Dennison J.R., Phys.Rev.Lett.64, 764 (1990)
14 Frank V.L.P., Lauter H.J., Godfrin H. and Leiderer P.,"Phonons 89", Hunklinger. S., Ludwig W. and Weiss G.edts.(World Scientific, Singapore 1990) p.1001

15 Butler D.M., Litzinger J.A. and Steward G.A., Phys.Rev.Lett.44, 466 (1980)
16 Chan M.H.W., Migone A.D., Miner K.D. and Li Z.R., Phys.Rev.B.30, 2681 (1984)
17 Kim H.K., Zhang Q.M.and Chan M.H.W., Phys.Rev.B 34, 4699 (1986)
18 Ni X.Z. and Bruch L.W., Phys Rev.B 33, 4584 (1986)
19 Hakim T.M., Glyde H.R. and Chui S.T., Phys.Rev.B 37, 974 (1988)
20 Frank V.L.P., Lauter H.J., Godfrin H. and Leiderer P.,"Phonons 89", (World Scientific, Singapore 1990) p.913
21.Frank V.L.P, Lauter H.J. and Leiderer P., Jap.J.Appl.Phys.26, 347 (1987),(Proc.18th Int.Conf.on Low Temperature Physics, Kyoto)
22.Kosterlitz M. and Thouless D.L., Prog in Low Temp.Phys. VII B, 371 (1987)
23.Halpin-Healy T. and Kardar M., Phys.Rev.B 34, 318 (1986)
24.Hering S.V, Van Sciver S.W and Vilches O.E., J.Low Temp.Phys. 25, 793 (1976)
25.Motteler F.C, Thesis (Univ. of Washington, 1985)
26.Lauter H.J., Godfrin H., Frank V.L.P. and Schildberg H.P., LT-19, Physica B165&166, 597 (1990)
27.Lauter H.J.,Schildberg H.P., Godfrin H., Wiechert H.and Haensel R., Can.J.Phys. 65, 1435 (1987)
28.H.P.Schildberg, H.J.Lauter, H.Freimuth, H.Wiechert and R.Haensel, Jpn.J.Appl. Phys. 26, 343 (1987)
29.Keshishev K.O., Parshin A.Ya. and Babkin A.B., Sov.Phys. JETP 53, 362 (1981)
30.Edwards D.O. and Saam W.F., Prog. in Low Temp.Phys. VII A, 283 (1978)
31.Lauter H.J., Frank V.L.P., Godfrin H. and Leiderer P., Elementary Excitations in Quantum Fluids, Ohbayashi K and Watabe M. Eds.,Springer Series in Solid-State Sciences 79 (1989) p.99
Lauter H.J., Godfrin H. and Wiechert H., in "Phonon Physics",Kollar J.et. al. edts., (World Scientific, Singapore 1985) p.842
32.Godfrin H., Frank V.L.P., Lauter H.J. and Leiderer P.,"Phonons 89", Hunklinger. S., Ludwig W. and Weiss G.edts.(World Scientific, Singapore 1990) p.904
33.Lauter H.J., Godfrin H., Frank V.L.P. and Leiderer P., NATO Workshop, Exeter 1990